THE JOURNAL OF PHYSICAL CHEMISTRY C

ARTICLE

pubs.acs.org/JPCC

Heterogeneous Photocatalytic Remediation of Phenol by Platinized Titania−Silica Mixed Oxides under Solar-Simulated Conditions

Harrison S. Kibombo* and Ranjit T. Koodali*

Department of Chemistry, University of South Dakota, Vermillion, South Dakota 57069, United States

ABSTRACT: Aperiodic mesoporous TiO_2−SiO_2 mixed oxide materials were platinized by the incorporation of Pt^0 by three different methods to understand the role of Pt on the photocatalytic activity of phenol under solar simulated conditions. The physicochemical properties of the resultant photocatalysts were examined by powder X-ray diffractometry, nitrogen adsorption, diffuse reflectance spectroscopy, and transmission electron microscopy. These characterization techniques illustrated the enhanced morphological properties of the mesostructure such as the presence of highly crystalline anatase TiO_2, large pore geometries, and active Ti−O−Si linkages, respectively. CO chemisorption analysis and TEM images accentuated the role of small Pt crystallite sizes in the development of photocatalysts with high degradation efficiencies.

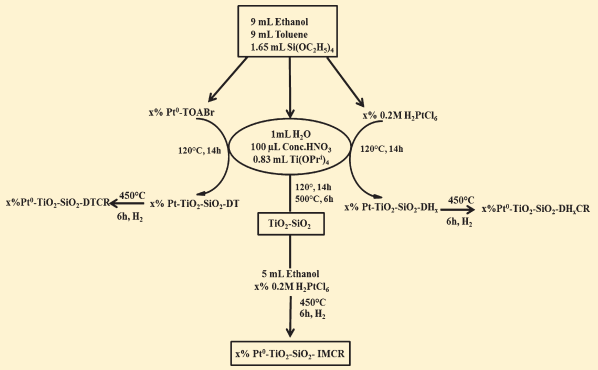

1. INTRODUCTION

The release of untreated waste streams from industrial, mining, and manufacturing activities results in the accumulation of persistent organic pollutants (POPs) and their derivatives in the environment. Prolonged exposure to high concentrations of such organic compounds poses an imminent threat to health and plays a significant role in enabling cardiovascular related diseases in humans.[1−4] Therefore, it is imperative to curb and minimize the prevalence of these pollutants and such processes may require using efficient preventative and remediation methods. Existing technologies for wastewater treatment are based on precipitation, microfiltration, flocculation, membrane reactors, and activated sludge processes; however, these techniques are highly energy-intensive, inefficient, and costly because the detoxification processes rely on multiple steps for the release of desired innocuous products and generate large amounts of secondary wastes. These challenges have prompted numerous studies to develop novel technologies for the complete mineralization of toxic organic pollutants in a limited time and at low cost.

In recent years, innovative research for the development of advanced products has realized nanomaterials that demonstrate the unique structural, mechanical, optical, electronic, and catalytic properties under light irradiation.[5] Despite the superior features of photostability and low cost,[6] the activity of TiO_2 photocatalyst is limited to the UV region, and the semiconductor is prone to recombination of charge carriers. Several techniques have been investigated to enhance the ability of TiO_2 to ensure prolonged lifetime of electronic charge carriers and impart enhanced photocatalytic activity. The use of precious metals such as Pt, Pd, Ag, Au, and Rh[7] in the photocatalyst matrix is promising because of their high electron affinity that minimizes electron−hole recombination, and shifts the spectral response into the visible region. This intimate contact between the metal and semiconductor assists in the rapid scavenging of excited electrons in the conduction band of the bulk photocatalyst, thus creating a Schottky barrier that minimizes the recombination of electron−hole pairs, and as a result the photocatalytic performance is often enhanced.[8] Pt is the precious metal of choice in this study because of its photostability, and possesses different valence states that show remarkable catalytic activity for a variety of organic reactions such as hydrogenation, and cracking of hydrocarbons.[9] The role of platinum in enhancing activity is still a major source of debate in mesoporous material research. Studies by Emilio et al. indicate a trivial effect of Pt on the activity of Degussa P25 due to the two phase composition that already provides an efficient suppression of charge carrier recombination.[10] Sun and coworkers have platinized rutile TiO_2; however, the reduced mobility and diffusivity facilitate the recombination of electrons and holes in rutile,[11] thus limiting the number of electrons transferred to O_2 to create photocatalytically reactive oxygen species.

Some investigators have opted to utilize economical supports such as SiO_2 and Al_2O_3 onto which TiO_2 particles can be dispersed to increase the availability of electrons and holes that participate in oxidative reactions. The incorporation of an amorphous phase is necessary to minimize the agglomeration of TiO_2 particles at high calcination temperatures. SiO_2 is a good candidate for this purpose because of its uncharged framework and moderate hydrophobicity allowing preconcentration of the organic material on the photocatalyst surface. Intricate procedures such as coprecipitation, flame hydrolysis, impregnation, and chemical vapor deposition have indicated that the interaction

Received: October 6, 2011
Revised: November 18, 2011
Published: November 28, 2011

of TiO_2 with SiO_2 generates a material with new catalytically active sites, possessing enhanced photostability due to the presence of the supporting SiO_2 phase.[12,13] In a previous study, we have reported highly active TiO_2-SiO_2 mixed oxide photocatalysts prepared using sol−gel chemistry because it allows versatility in tuning the physicochemical properties of the inorganic oxides during the preparation process.[14−16] Simple aromatic nonpolar cosolvents were utilized in the synthesis route to obviate the use of hybrid polymers,[17] alkoxide bridging ligand complexes,[18,19] and structure-directing agents that result in materials containing traces of residual ion impurities, which retard photocatalytic activity.[20,21] Such cosolvents increase the viability of reconstruction of pores by enhancing coordination expansion through the donation of π-electrons to titanium, slowing down its hydrolysis and improving molecular mixing of precursors. Our research indicates a higher activity of titania-based mixed oxides (TiO_2-SiO_2 in 1:3 ratio) compared with TiO_2, with TOC degradation efficiencies greater than 90% under UV irradiation, owing to three synergetic factors, that is, the availability of active sites by optimizing the anatase content, the utilization of suitable cosolvents to enhance dispersion of anatase in the silica framework, and the ability of the combination of the hydrothermal synthesis and optimum calcination temperature to maximize the crystallinity of the anatase species.[22]

In this work, we introduce Pt species into mesoporous TiO_2-SiO_2 by three simple approaches, direct infusion, template, and impregnation, to establish the best method suitable for the synthesis of highly active precious-metal-loaded mixed oxides for the degradation of organic pollutants such as phenol under solar-simulated conditions. Hydrothermal treatment was imparted to achieve highly stable crystalline materials in a limited period of time of <1 day. The effective control of crystallite sizes is under active scrutiny, and of the work published, none to the best of our knowledge illustrates a comparative study of different methods that achieve Pt in highly crystalline TiO_2-SiO_2 for the degradation of phenol, with their optimum particle sizes. During the remediation by heterogeneous photocatalysis, reactive oxygen species (ROS) such as $^{\bullet}OH$ and $O_2^{\bullet-}$ radicals are generated.[23,24] These species have the ability to disintegrate the phenol molecule by substituting into the aromatic ring to form a quinone or attack C−C bonds to form a carbonyl or even oxidize the alcohol and carbonyl groups to form carboxylic acids that eventually undergo a series of C−C bond fragmentation until all carbon atoms of the organic molecule are transformed into their highest oxidation state, that is, CO_2.

2. EXPERIMENTAL METHODS

2.1. Materials. Commercially available titanium isopropoxide $Ti[OCH(CH_3)_2]_4$ ($Ti(OPr^i)_4$, Acros, 98+%), tetraethylorthosilicate $Si(OC_2H_5)_4$ (TEOS, Acros, 98%), methanol (Acros, 99.9% HPLC grade), ethanol (Pharmco-AAPER, A.C.S/USP grade, anhydrous), hydrogen hexachloroplatinate (IV) hydrate H_2PtCl_6 (Acros, ACS grade), potassium tetrachloroplatinate (II) K_2PtCl_4 (Pressure Chemical), tetra-*n*-octylammonium bromide $[CH_3(CH_2)_7]_4N$ Br (TOABr, Alfa Aesar, 98+%), sodium borohydride powder $NaBH_4$ (Acros, 98+%), 4-dimethyl-aminopydridine $(CH_3)_2NC_5H_4N$ (DMAP, Acros, 99%), toluene (Acros, ACS grade), conc. nitric acid HNO_3 (Acros, ACS grade), phenol (PhOH, Acros, 99+%, ACS grade), hydroquinone (HQ, Sigma, >99%), 1,2,4 benzenetriol (Aldrich, 99%), pyrogallol (PG, Alfa Aesar, 99% packed under argon, ACS grade), fumaric acid (FA, Acros, 99+%), maleic acid (MA, Alfa Aesar, 98+%), and Aeroxide TiO_2 P25 (Evonik Degussa) were used as such. Deionized water (resistivity > 18 MΩ-cm) was used for dilution throughout this study, and the chemicals mentioned above were used without further purification. Benzoquinone (BQ, TCI America, 98%) was purified by heating in an evaporating dish covered with a glass funnel and externally lined with Whatmann filter paper. The compound sublimes and sticks to the inner walls of the funnel as bright yellow crystals.

2.2. Synthesis of Mesoporous Gels. The $Pt-TiO_2-SiO_2$ mixed oxide catalysts utilized in this study were prepared by simultaneous hydrolysis and condensation of metal alkoxides, TEOS and $Ti(OPr^i)_4$ by the sol−gel method, with emphasis on the method of incorporation of Pt complexes into the TiO_2-SiO_2 mesostructure. Three different approaches were employed, namely; direct infusion (DHxCR), template (DTCR), and impregnation (IMCR). For the DTCR method, performed Pt nanoparticles were first synthesized by the variation of a method reported by Garcia-Martinez and coworkers[25] constituting the reduction of $[PtCl_4]^{2-}$ by $NaBH_4$ in the presence of tetra-*n*-octylammonium bromide (TOABr) acting as a capping agent. TOABr (1.1 g, 50 mM) was dissolved in a mixture of 13.0 mL of 34.6 mM K_2PtCl_4 and 40 mL of toluene and stirred at 300 rpm for 1 h. The transfer of $[PtCl_4]^{2-}$ to the organic phase was evidenced by the red-brown color and confirmed by an absorption peak in the UV spectrum due to the presence of Pt complex anions. The aqueous phase was eliminated and the organic phase was dried with anhydrous Na_2SO_4. Freshly prepared 0.1 M $NaBH_4$ (8−12 mL) was added dropwise without sintering and stirred at 300 rpm overnight. The mixture was washed three times with 40 mL of H_2O and then once sequentially with 40 mL of 0.1 M H_2SO_4, 40 mL of 0.1 M NaOH, and another 40 mL of H_2O. The resultant organosol was dried with anhydrous Na_2SO_4 and decanted to a beaker. 4-Dimethylammonium pyridine (DMAP, 0.122 g) was dissolved in 10 mL of H_2O, added to the organosol, and stirred for 2 h. UV−vis spectra of the organic and aqueous phases were obtained to confirm the location of Pt ions in the organic phase by a strong peak at 288 nm. The Pt ions were observed to have remained in the TOABr phase and denoted as Pt-TOABr.

Platinum complex solutions were then incorporated into the TiO_2-SiO_2 mesostructure through a sol gel route. In a typical synthesis, 1.65 mL of TEOS was added slowly to a solution of 9 mL of toluene and an appropriate amount of platinum containing solution dissolved in 9 mL of C_2H_5OH (200 proof, anhydrous) under vigorous stirring in three separate Teflon linears. Portions of Pt-TOABr corresponding to 0.5, 1, and 2 wt % were added to each liner. The DHxCR method proceeds through a similar route in separate liners, but at this stage, direct infusion of 86 μL, 0.17 mL, and 0.34 mL of 0.2 M H_2PtCl_6 solution is carried out to achieve 0.5, 1, and 2 wt % Pt, respectively. For the two methods, the hydrolysis process was initiated by the introduction of 1 mL of H_2O and catalyzed by the addition of 100 μL of conc. HNO_3. $Ti(OPr^i)_4$ (0.83 mL) was added dropwise, and the suspensions were left to stir for 3 h to enhance homogeneity and gelation. The resultant gels were subjected to hydrothermal treatment in a Thermolyne autoclave reactor furnace and heated to a temperature of 120 °C for 14 h, filtered, and dried overnight at 70 °C.

The third method involved the preparation of TiO_2-SiO_2 (TiO_2/SiO_2 1:3) using a similar approach as discussed without the inclusion of Pt complex solutions. The resultant powder was divided into three 0.5 g portions. The photocatalysts were wetted with 5 mL of ethanol in Nalgene beakers and stirred vigorously

Scheme 1. Flow Chart Illustrates a Sol Gel Route through Which Three Different Experimental Approaches Can Be Utilized to Prepare Pt−TiO_2−SiO_2 Mixed Oxide Materials[a]

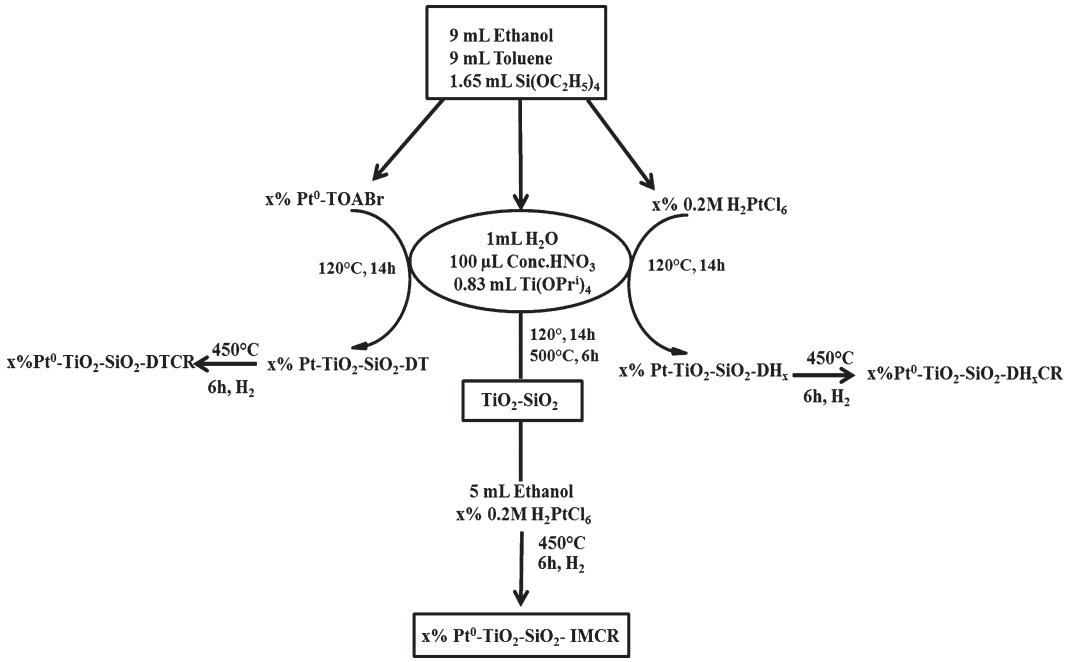

[a] Direct infusion, template, and impregnation are denoted as DHxCR, DTCR, and IMCR.

for 10 min. We then added 86 μL, 0.17 mL, and 0.34 mL of 0.2 M H_2PtCl_6 to the individual beakers to obtain 0.5, 1, and 2 wt % platinum impregnation, respectively. The suspensions were left to dry overnight at ambient temperature prior to reduction under H_2 flow.

The powders obtained from the three synthesis methods were ground and calcined at 450 °C under H_2 flow for 6 h at a heating rate of 3 °C/min as an efficient means of reducing Pt species to their metallic state (Pt^0) while maintaining the morphology of the platinum particles. The syntheses procedures are summarized in Scheme 1.

2.3. Characterization of Pt−TiO_2−SiO_2. The calcined samples were characterized by X-ray powder diffraction using a Rigaku Ultima IV with PDXL software. The diffraction patterns were recorded at room temperature employing Ni-filtered Cu Kα radiation (λ = 1.5408 Å), an accelerating voltage of 40 kV, and emission current of 44 mA. The angle regions were scanned from 20 to 80°(2θ) with a step size of 0.02°. The textural properties such as surface area and pore size distribution of the mixed oxide materials were measured using N_2 physisorption measurements. After the samples were dried overnight at 70 °C and degassed at 100 °C for at least 1 h, N_2 adsorption−desorption isotherms were obtained at 77 K using a NOVA 2200*e* (Quantachrome Instruments) surface area and pore size analyzer. The surface areas were calculated by using the Brunauer−Emmett−Teller equation within a relative pressure range (P/P_0) of 0.05 to 0.30. The pore volume was determined from the amount of nitrogen adsorbed at the highest relative pressure of $P/P_0 \approx 0.99$. The pore diameter was determined by applying the Barrett−Joyner−Halenda (BJH) model to the desorption isotherm. The UV−vis diffuse reflectance (DR) spectra of the samples were recorded in the range of 210−600 nm using a Cary 100 Bio UV−vis spectrophotometer equipped with a Harrick DR praying mantis accessory. Fourier transform infrared (FT-IR) spectroscopy studies were initiated by drying the materials in the oven overnight at 70−80 °C to eliminate moisture. The infrared spectra of the Pt−TiO_2−SiO_2 materials were recorded using a Bruker instrument model ALPHA equipped with ATR Diamond module of spectral range capabilities from 50 000 to 50 cm^{-1}. The crystal type is automatically recognized by the spectroscopy software OPUS 6.5, and optimal measurements were obtained at 24 scans and 4 cm^{-1} resolution. Transmission electron microscopy (TEM) images were recorded on a Tecnai G^2 instrument operating at accelerator voltage of 120 kV. The sample for TEM studies was prepared by suspending Pt−TiO_2−SiO_2 in ethanol and sonicating for 1 h. A drop of the suspension was cast on the copper grid coat containing a carbon film and allowed to dry overnight in a Petri dish prior to collecting images. CO pulse chemisorption was carried out using the CHEMBET-3000 TPR/TPD (Quantachrome Instruments) at ambient temperature and pressure. All materials and quartz U-tube were dried at 70 °C overnight prior to analysis. An adsorbate and carrier gas flow of 90 mL/min and heating rate of 10 K/min were maintained throughout the course of the experiment. Typically, 90−100 mg of material was loaded into the U-tube, outgassed at 130 °C for 1 h under He flow, and then cooled to room temperature. After switching the gas to H_2 and stabilizing the flow, the material was reduced at 350 °C for 2 h and cooled to room temperature again. The flow gas was switched back to He, and CO gas was introduced through the calibration titration valve. The thermal conductivity detector (TCD) signal was stabilized at an attenuation of 8 and detector current of 150.0 mA by using the coarse and fine adjustment knobs. CO pulses (100 μL each) were injected into the carrier gas until the surface of the material was saturated. The TCD responded to the quantity of adsorbate that was not chemisorbed hence the

platinum dispersion, and particle size measurements were calculated by pulse titration analysis generated by Quantachrome TPRWin v2.1 software. The amounts of Pt in the Pt−TiO_2−SiO_2 mixed oxide catalysts were determined by inductively coupled plasma mass spectrometry (ICP-MS). Samples were accurately weighed (∼ 0.025 g) and digested with 5 mL of HNO_3 and 5 mL of HCl and then diluted to 50 mL. The concentration of Pt in the samples was determined from a previously made calibration plot. The amount of Pt determined by ICP-MS was estimated to be almost identical to the initial amount used in the synthesis gel, indicating good retention of Pt in the TiO_2−SiO_2 mixed oxide materials.

2.4. Photocatalysis Experiments Using Pt−TiO_2−SiO_2 Materials. The photocatalytic activity of the prepared Pt−TiO_2−SiO_2 mixed oxide catalysts was assessed by monitoring the degradation of phenol from aqueous suspensions. 100 mg of catalyst were dissolved in 100 mL of phenol solution (2×10^{-4} M) in a quartz cylindrical jacket reactor at initial pH of 4 to 5. The suspensions were stirred at a rate of 300 rpm in the dark for 0.5 h to ensure adsorption−desorption equilibrium and purged with molecular oxygen at ∼60 mL/min. The reaction temperature was kept constant at ∼25 °C by channeling water though the double-walled reactor. Irradiation for 3 h was carried out by a Xenon lamp (Newport 1000 W) through a Pyrex glass cut filter of 280 nm. These experimental conditions were maintained throughout the course of the experiment, and 15 mL aliquots were collected every 30 min. Each suspension was centrifuged at 3200 rpm for 15 min and filtered through a 0.45 μm Millipore filter membrane, and the clear solutions were analyzed as described in the following sections.

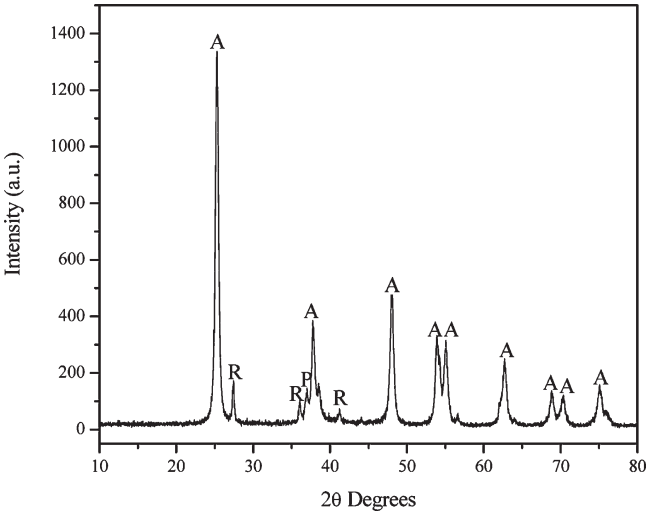

Figure 1. Powder X-ray diffraction patterns of Pt−TiO_2-2% showing the formation of mixed phases of anatase (A) and rutile (R) along with peaks due to the presence of platinum (P) in the mesostructure.

2.5. Degradation Efficiencies of Pt−TiO_2−SiO_2 Materials. The amount of organics remaining in solution was estimated using a Shimadzu TOC-V CSH total organic carbon analyzer immediately after filtration to confirm the catalytic activity of the mixed oxides. Also, post-photocatalysis, identification and quantification of unreacted phenol and its reaction intermediates was carried out by high-performance liquid chromatography (HPLC) using a Spectra-Physics 8800 chromatograph equipped with an Alltech Ultrasphere C-18, 5 μ long reverse phase column of 250 mm length, internal diameter of 4.6 mm, and Spectra 100 Variable wavelength detector. The eluents consisted of a methanol/water mobile phase composition of 40:60 by volume (containing 1 vol% acetic acid) at a flow rate 1 mL/min and were detected at a wavelength of 254 nm.

Stock solutions of desired concentrations of HQ, PhOH, BQ, FA, PG, catechol (CC), and 1,2,4-benzenetriol (HHQ) were prepared in deionized water for the identification of phenol intermediates. Calibrations plots were derived from the solutions diluted to concentrations of 2×10^{-5}, 5×10^{-5}, 1×10^{-4}, and 2×10^{-4} M and purged with argon to minimize autoxidation.

3. RESULTS AND DISCUSSION

3.1. Structural Effects of Platinum on TiO_2 prepared by Cosolvent Induced Gelation. The powder XRD of Pt−TiO_2 was investigated prior to their dispersion into the amorphous SiO_2 phase to understand the effect of the support on the activity of Pt species in these mesoporous materials. Figure 1 illustrates powder X-ray diffraction patterns of a highly crystalline TiO_2 material prepared by cosolvent induction of toluene and loaded with 2 wt % platinum by the direct addition of H_2PtCl_6 into the sol−gel synthesis route. A diffraction peak (P) at 37.1° (2θ) was

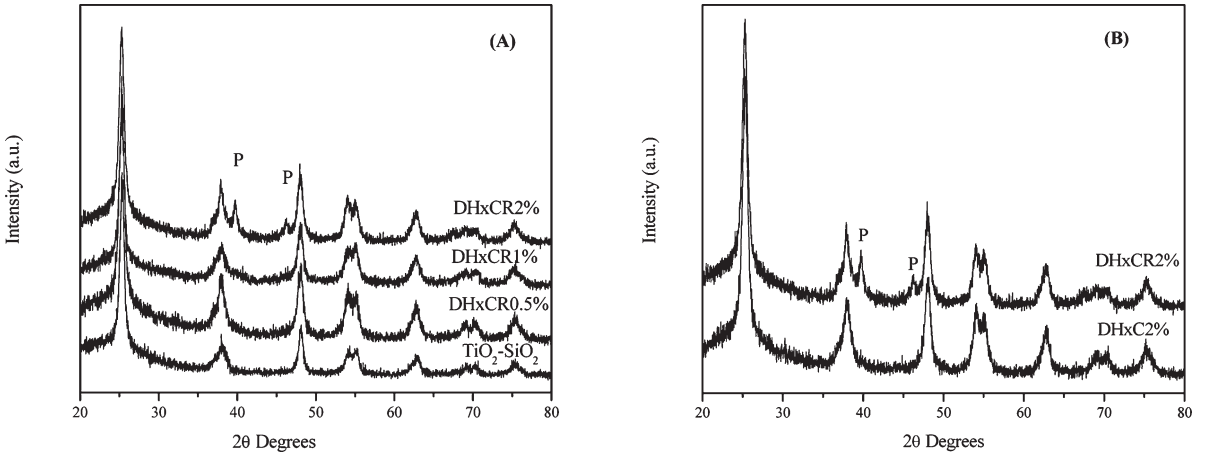

Figure 2. Powder X-ray diffraction patterns of Pt−TiO_2−SiO_2 materials synthesized by the direct incorporation of H_2PtCl_6 into the synthesis sol (direct method). (A) XRD of Pt−TiO_2−SiO_2 (DHxCR) materials with Pt loadings of 0.5, 1, and 2 wt % and (B) calcined Pt−TiO_2−SiO_2 (DHxC2%) prior to reduction and Pt−TiO_2−SiO_2 (DHxCR2%) after reduction.

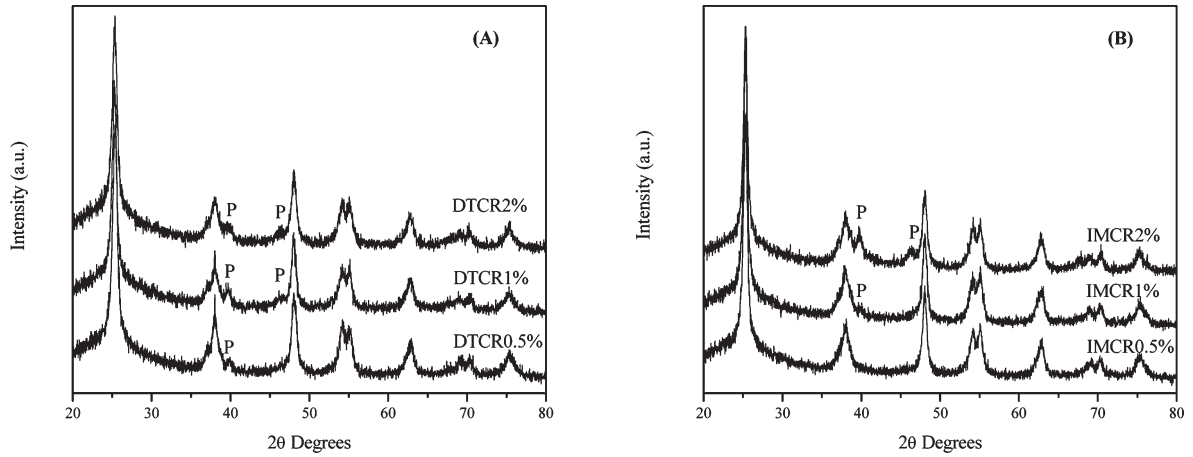

Figure 3. Powder X-ray diffraction patterns of Pt−TiO_2−SiO_2 materials synthesized with: (A) different Pt wt % loadings of 0.5, 1, and 2 wt % by using (A) preformed Pt-capped with TOABr and (B) by impregnation of H_2PtCl_6 on previously prepared TiO_2−SiO_2, followed by reduction of the Pt ions at 450 °C under H_2.

observed, indicating the presence of Pt in the TiO_2 materials. It is notable that high contrast peaks of mixed phases of both anatase (A) and rutile (R) were observed in this sample. However, the incorporation of a SiO_2 support results in lower contrast anatase peaks and the disappearance of the peaks due to rutile phases, as illustrated in Figure 2.

High-angle X-ray diffractograms of calcined materials of unplatinized TiO_2−SiO_2 juxtaposed to 0.5, 1, and 2 wt % Pt loadings denoted as DHxCR0.5%, DHxCR1%, and DHxCR2% prepared by the addition of Pt precursor, H_2PtCl_6, using the direct method and then reduced at 450 °C are shown in the Figure 2A. The samples exhibit diffraction peaks due to d_{101}, d_{004}, d_{200}, d_{105}, and d_{204} at two θ values of 25.2, 37.9, 48.1, 55.1, and 62.8°, respectively, indicating that the materials possess only the anatase phase of TiO_2. Unplatinized TiO_2−SiO_2 results in distinct peaks of the anatase phase of TiO_2 showing a diffraction contrast similar to that of the Pt-loaded TiO_2−SiO_2 materials, suggesting high crystallinity for all catalysts prepared in this study. The anatase phase is dominant in the DHxCR0.5% and DHxCR1%, obscuring the Pt peaks due to their low amounts or effective dispersion in the highly amorphous silica phase or occlusion of scattering by the amorphous SiO_2 phase. Additive loadings of Pt to obtain DHxCR2% show a gradual emergence of peaks at 41 and 46° (2θ). The presence of Pt species in the meso-matrix was confirmed by comparative diffractograms of a material calcined in air to that reduced under H_2 flow, as shown in the Figure 2B. The peaks are indexed by the PDXL software and are matched for Pt^0 reiterating the ability of H_2 to reduce Pt species such as PtO_2 and PtO to Pt^0. Under similar reduction conditions, the TiO_2−SiO_2 materials resulting from the incorporation of preformed Pt capped with TOABr, exhibited diffraction peaks of the anatase phase, mainly as illustrated in Figure 3A. Diffraction peaks due to Pt^0 species were also observed in all loading ratios in these samples, suggesting larger crystallite sizes (see discussion later).

Similar trends were achieved with the materials prepared by the impregnation method, as illustrated in the Figure 3B with Pt peaks more prominent in the diffractogram for the material, IMCR2%.

The nitrogen isotherms of the Pt−TiO_2−SiO_2 mixed oxides prepared by the three synthesis methods were examined, and they exhibit type IV isotherms that are characteristic of mesoporous materials. At low relative pressures, the initial part of the type IV isotherm is ascribed to monolayer adsorption, and as the relative pressure increases, multilayer adsorption occurs prior to capillary condensation. This structural property is evident mainly in the materials prepared by the DHxCR method at 0.5 and 1 wt % Pt-loadings, as depicted in the Figure 4A. An increase in Pt loading to 2 wt % resulted in a material of Type V isotherm that is convex in nature over the entire range of relative pressure, suggesting that the lateral interactions between adsorbed molecules are relatively stronger than the interactions between the adsorbent surface and adsorbate.

The other synthesis methods, that is, DTCR and IMCR (not shown for clarity) resulted in materials of adsorption isotherms similar to that of DHxCR2% irrespective of the Pt-loading. The adsorption−desorption isotherms of mesoporous materials exhibit a characteritic feature called hysteresis arising from network effects such as differences in porosities that cause independent occurrences of filling and emptying of pores. Larger pores that may need to access the structural environment through smaller pores will empty at pressures coinciding with those necessary for capillary evaporation of the smaller connecting pores.[26] All materials prepared in this study displayed hysteresis loops of H3 type classification without leveling off at relative pressures close to the saturation vapor pressure, suggesting that the materials are composed of loose assemblages of irregular shaped plate-like particles forming slit-like pores of broad pore size distribution.[27] The desorption branch of these mixed oxides contains a modest region associated with gradual closure of the loop, implying a delayed evaporation of the adsorbate. These isotherms exhibit unique pore size characteristics, and Figure 4B shows distributions of corresponding materials. DHxCR0.5% results in a hierarchically ordered set of pores with micro-, meso-, and macroparticles centered at 21, 39, and 67 Å, respectively. A bimodal distribution of pores is achieved with an increase in the Pt-loading. DHxCR1% exhibits sets of pores averaging at 35 and 97 Å, whereas DHxCR2% consists of pores in the region of 35 and 168 Å. It is evident that although all materials exhibit H3 type hysteresis, the amount of adsorbate adsorbed varies due to the differences in porosities and a resultant difference in surface areas is obtained. The preparation procedure determines the difference

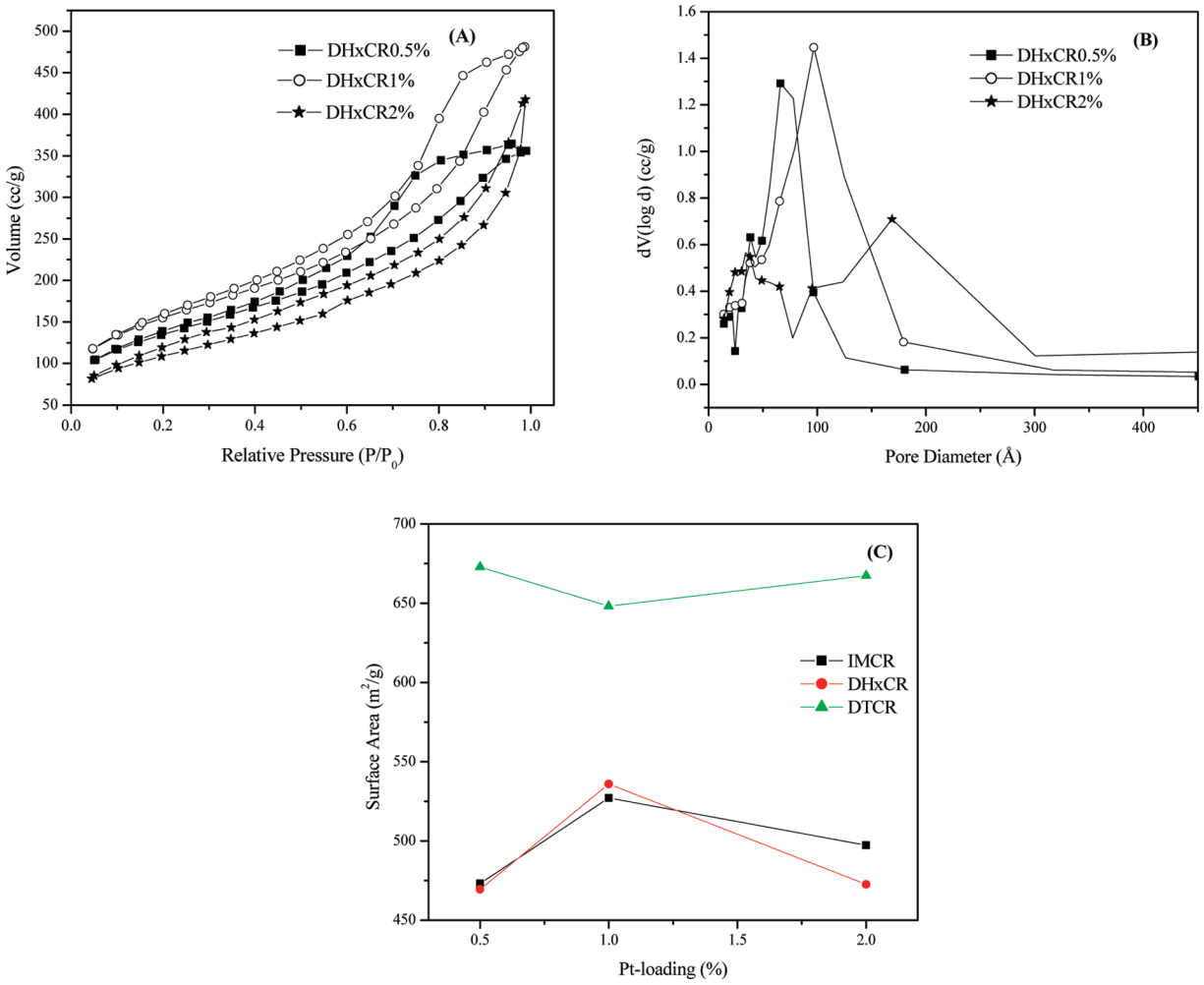

Figure 4. Variation in surface areas of $Pt-TiO_2-SiO_2$ materials synthesized with different Pt wt % loadings of 0.5, 1, and 2% by the DHxCR method. (A) Adsorption−desorption isotherms, (B) pore size distribution curves, and (C) plot of surface area versus Pt-loading comparing the three different synthesis methods, DHxCR, DTCR, and IMCR.

in textural features of the resultant photocatalysts. The incorporation of 0.5 wt % Pt using the DHxCR and IMCR methods results in a reduction in surface area from 671.5 to 496 and 473 m^2/g, respectively, as depicted in Figure 4C. The surface areas decrease because of agglomeration of Pt in the support through microvoids and defects that block their access to adsorbate molecules.[28,29] An increase in Pt loading to 1% results in unique scenarios for the two synthesis methods. The DHxCR method involves the incorporation of Pt ions in the synthesis route prior to hydrothermal treatment, thus facilitating their access to the pores of the mesostructure. We observe an increase in surface area due to lesser agglomeration depicted by the reduction in average crystallite sizes from 17 to 12 nm. The addition of more Pt to 2% results in a decrease in surface area because more Pt can access and block the pores. A similar trend was observed when the impregnation method (IMCR) is employed, however, with an increase in crystallite size noted. It is likely that noble metal deposition at 1% was achieved more on the surface than in the pore cavities of the material. Although, incorporation of preformed Pt is through the sol gel synthesis route, the DTCR method appears to have subtle effect on the surface area irrespective of the amount of Pt. The relatively high pore volumes suggest that the surfactant-stabilized Pt crystallites may be anchored on surface of the interstitial spaces, leaving the pores accessible to diffusion of adsorbate molecules. The diffusion of Pt species into these cavities of the support causes a narrowing of the pore diameter and blocking some of the pores.[30,31] An increase in Pt loading up to 2% results in a slight decrease in the surface area from 673 to 667 m^2/g. This may be attributed to the average growth in the size of platinum from 24.5 to 27.9 nm that narrows the average pore diameter from 71 to 45 Å depicted by the chemisorption and surface area analyses, respectively, in Table 2. A summary of the textural properties, including specific surface area, pore volume, and average pore diameter, obtained from nitrogen adsorption−desorption analysis is shown in the Table 1.

Light absorptive properties of the $Pt-TiO_2-SiO_2$ materials were investigated using UV−vis DR spectroscopy. The materials exhibited an absorption below 400 nm primarily attributed to excited electron transitions from the valence band to conduction band of the anatase TiO_2 semicondutor, as illustrated in the Figure 5. Unplatinized TiO_2-SiO_2 featured absorption at slightly larger wavelength than the Pt-loaded materials, with an effective bandgap energy estimated at 3.33 eV by extrapolation of the linear portion of the spectrum to zero absorption. The incorporation of Pt into the mesostructure resulted in a slight

dx.doi.org/10.1021/jp209620j |J. Phys. Chem. C 2011, 115, 25568–25579

blue shift, inferring a change in the crystallite size of the anatase TiO_2 and higher estimates of the effective bandgap were achieved in the range of 3.45 to 3.64 eV. The blue shift was most prominent in the 2% Pt-loaded materials for the three synthesis methods studied, probably due to a change in dispersion, that is, the higher loading (less matrix TiO_2) resulting in a high dispersion of anatase.[32]

Information on the lattice vibrations of the Pt−TiO_2−SiO_2 mixed oxide materials is provided by IR spectroscopic studies (not shown). The most intense band in the spectrum appearing at 1066 cm^{-1} is assigned to asymmetric mode of Si−O−Si stretching vibration with bridging oxygen,[33,34] and this band is not observed in the Pt−TiO_2-2%, confirming the absence of the SiO_2 phase. Symmetric vibrations and associated deformation modes of SiO[35] are detected within the broad range of 800 and 596 cm^{-1}, respectively. The possible interaction between TiO_2 and SiO_2 at molecular level is evidenced by a weak band at 953 cm^{-1}, which may be associated with the Ti−O−Si hetero linkages.[33,36] This band is of significantly lesser intensity for the DHxCR and IMCR methods but is most pronounced for the DTCR synthesis method. The strong Ti−O−Ti absorption at 444 cm^{-1} is due to crystalline titania that is further evidenced by the lattice fringes in the TEM images discussed later. The adsorbed CO_2 may dissociate on Pt to form CO and oxygen,[37] resulting in band traces around 2181 cm^{-1} that suggest interaction between CO and TiO_2.[38] The very weak adjacent bands at ∼2094 cm^{-1} have been ascribed to CO adsorbed to metallic Pt^0.[39] Weak absorption characteristics of the scissor bending mode of physisorbed water are evidenced by a band at 1640 cm^{-1}, whereas the vibration at 3388 cm^{-1} is ascribed to a deformation mode of molecular H_2O.[40] This band is broad in the unplatinized TiO_2−SiO_2 and appears to disappear in the Pt-loaded materials probably due to the absence of sufficient surface hydroxyl groups. The broad adsorption band between about 2900 and 3700 cm^{-1} corresponds to the fundamental stretching vibrations of surface hydroxyl groups emerging from SiO-H, TiO-H, and TiO-H_2O species vibrating at 3200 and 3400 cm^{-1}, respectively, due to O−H stretching of hydrogen bonded molecular water.[41,42]

Table 1. Textural Properties of Pt−TiO_2−SiO_2 Mixed Oxide Materials[a]

material	S_{BET} ($m^2\ g^{-1}$)[b]	pore volume ($cm^3\ g^{-1}$)	ave. pore diameter (Å)
Pt−TiO_2-2%	52.6	0.17	134.0
TiO_2−SiO_2	671.5	1.61	95.94
DHxCR0.5%	469.4	0.73	46.44
DHxCR1%	535.9	0.74	55.56
DHxCR2%	472.6	0.66	55.75
DTCR0.5%	672.8	1.18	70.60
DTCR1%	648.1	1.15	71.30
DTCR2%	667.4	0.75	44.81
IMCR0.5%	473.2	0.47	28.73
IMCR1%	527.2	0.83	62.88
IMCR2%	497.3	0.74	59.76

[a] Pt−TiO_2−SiO_2 samples are labeled according to synthesis method utilized to comprise of the direct (DHxCR), template (DTCR), and the impregnation (IMCR) method. The acronyms are followed by the wt % loading of Pt. [b] Surface area was determined by applying the Brunauer−Emmett−Teller (BET) equation to the adsorption isotherm.

3.2. Photocatalytic Efficiencies of the Pt−TiO_2−SiO_2 Materials. The structural characteristics and resultant photocatalytic efficiencies of platinized TiO_2-based materials depend on various parameters such as the Pt amount loaded, the oxidation state of Pt, the particle size, the dispersion of Pt, and the nature of the substrate degraded. The photocatalytic activities of Pt−TiO_2−SiO_2 materials were determined by total organic carbon (TOC) and LC analysis that estimates the amount of organics remaining in solution after the degradation reaction for up to 180 min. The results shown in Table 2 indicate clearly that the platinized materials demonstrate higher activities than unplatinized TiO_2−SiO_2 after 30 min solar simulated irradiation, thus emphasizing the role on platinum in enhancing the activity of mesoporous materials. Table 2 is representative of the high photocatalytic activity of our materials because irradiation for longer durations with especially the Pt-IMCR catalysts indicates complete degradation of phenol after 30 min. Powder XRD

Table 2. Summary of the CO Pulse Chemisorption and TOC Activity Results of the Pt−TiO_2−SiO_2 Mixed Oxide Materials Showing the Reaction Intermediates[a]

				intermediate concentration (ppm) from LC					
material	dispersion (%)	average crystallite size (nm)	TOC degradation 30 min (%)	MA	FA	PG	HQ	BQ	PhOH
Pt−TiO_2-2%	4.51	25.1	72	ND	ND	1.97	1.00	1.39	ND
TiO_2−SiO_2			9	ND	ND	1.22	ND	0.28	8.47
DHxCR0.5%	6.60	17.2	41	0.16	ND	1.52	1.52	0.64	ND
DHxCR1%	9.72	11.7	58	1.15	ND	1.67	1.34	0.13	ND
DHxCR2%	7.46	15.2	34	1.07	1.05	0.52	1.46	0.05	ND
DTCR0.5%	4.63	24.5	23	0.63	1.18	2.02	2.46	0.08	6.05
DTCR1%	5.13	19.8	16	1.12	1.87	2.47	2.41	0.19	9.49
DTCR2%	4.07	27.9	9	3.27	7.84	2.46	2.06	ND	3.65
IMCR0.5%	27.8	4.07	93	ND	ND	ND	ND	ND	ND
IMCR1%	20.5	5.54	93	ND	ND	ND	ND	ND	ND
IMCR2%	17.2	6.58	88	ND	ND	0.06	ND	ND	ND

[a] Pt−TiO_2−SiO_2 samples are labeled according to the synthesis method to comprise of the direct (DHxCR), template (DTCR), and impregnation (IMCR) method. The acronyms are followed by the calculated wt % loading of Pt. Initial concentration of phenol prior to photocatalysis is 15 ppm. *ND denotes compounds that are not detected. MA = maleic acid, FA = fumaric acid, PG = pyrogallol, HQ = hydroquinone, BQ = benzoquinone, and PhOH = phenol.

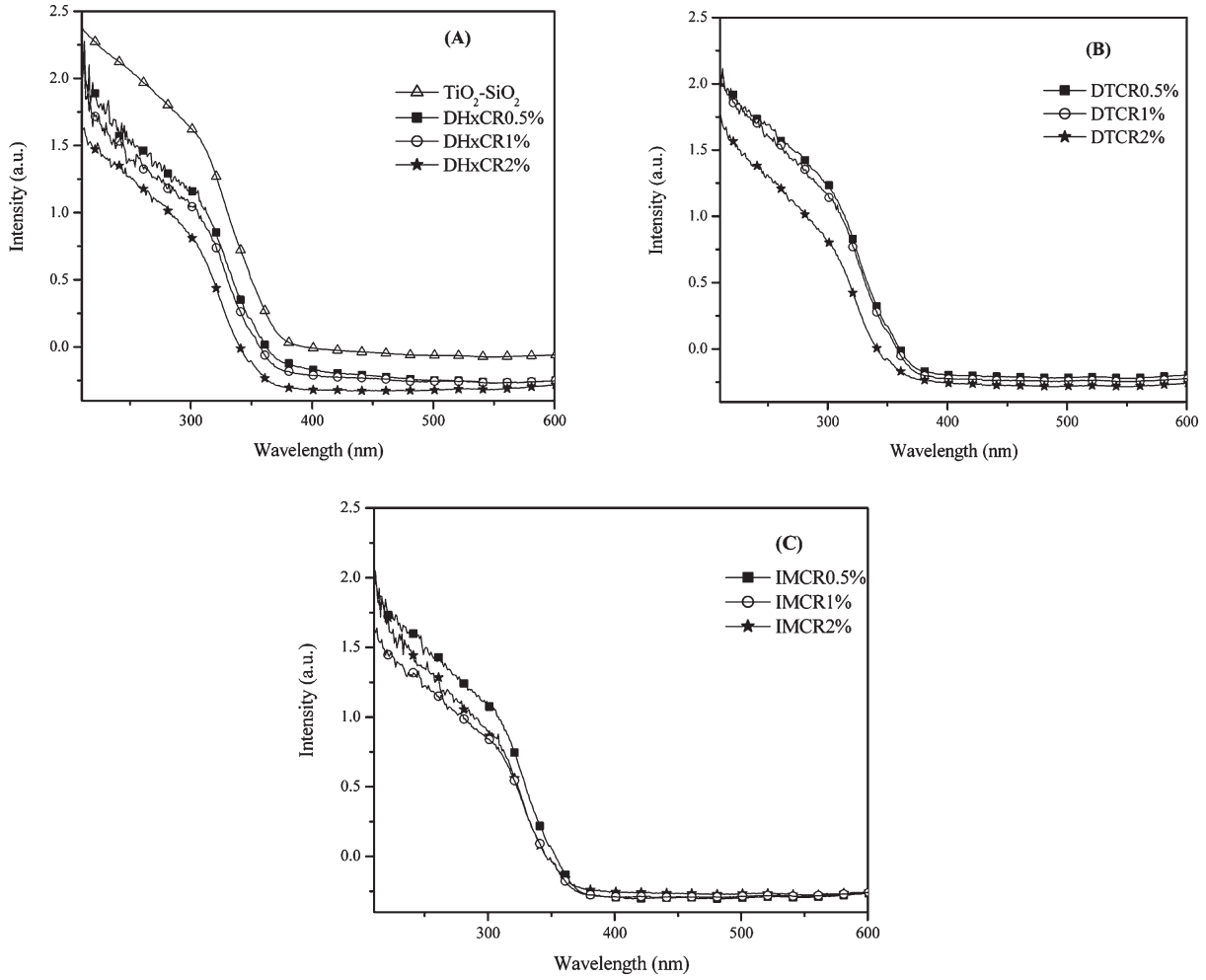

Figure 5. UV−vis diffuse reflectance spectra of Pt−TiO_2−SiO_2 materials with different Pt loadings of 0.5, 1, and 2 wt % synthesized by: (A) direct method (DHxCR), (B) template method (DTCR), and (C) impregnation (IMCR) method.

studies indicate that the crystallinity of the titania samples in the Pt- TiO_2−SiO_2 is similar, and thus we can try to determine other factors that are causing differences in the initial degradation rate of phenol after 30 min of irradiation. The dispersion of TiO_2 over amorphous SiO_2 may increase the diffusion length of electrons from the anatase crystallites to Pt particles, resulting into a slight decrease in photocatalytic activity at low Pt loading, that is, <1 wt %, as suggested by the degradation efficiencies. An increase in platinum loading to 2% on average resulted in a slight decrease in photocatalytic activity because catalytically active TiO_2 may be deprived of photogenerated electrons due to more competition with abundant Pt for UV photons.[32] Sun argues that the addition of more Pt lowers the electron density in the TiO_2 particles that results in a reduction of the electron density gradient. The electron flux through the Pt−TiO_2 contact reaches an equilibrium that negates the deposition of more Pt.[43] However, the purpose of this study is to devise a simple synthesis method that produces the most active platinized TiO_2−SiO_2 materials under solar simulated conditions. TiO_2−SiO_2 possesses a phenol degradation activity of 9%, and the introduction of Pt at 0.5 wt % by the DHxCR method causes an enhancement to 41%. The addition of more Pt species into the mixed oxide matrix to attain a 1 wt % loading results in a further improvement of the catalytic activity to 58% due to the ability of Pt to scavenge electrons and minimize charge-carrier recombination. However, the activity was retarded to 34% for material loaded at 2 wt % owing to agglomeration of Pt particles forming slightly larger crystallites, as evidenced in the CO chemisorption data discussed later.

In an alternative synthesis method, DTCR, Pt species were preformed by stabilization with TOABr and incorporated into the sol gel procedure. The material loaded with 0.5 wt % Pt exhibited a degradation efficiency of 23%, whereas an increase in Pt content to 1 and 2 wt % resulted in lower efficiencies of 16 and 9%, respectively. It is likely that the inclusion of more templated Pt-TOABr led to an occlusion of the active sites of the titania species, as evidenced in the obscurity of the titania fringes in the TEM images (discussed later). The deposition of Pt species into the TiO_2−SiO_2 matrix using the IMCR method is the most promising and efficient producing materials of enhanced photocatalytic activity under solar simulated conditions. The materials loaded with 0.5 and 1 wt % Pt possessed close to identical crystallite sizes of 4.1 and 5.5 nm, respectively, and as a result exhibited an equivalent degradation efficiency of 93%. Increasing the Pt content to 2% led to a slight decrease in activity to 88% due to a slight increase in the average particle size to 6.6 nm. We also observe that an optimum loading in the region of 1 wt % Pt produces the most active materials for both the IMCR and DHxCR synthesis methods. Considering that each synthesis

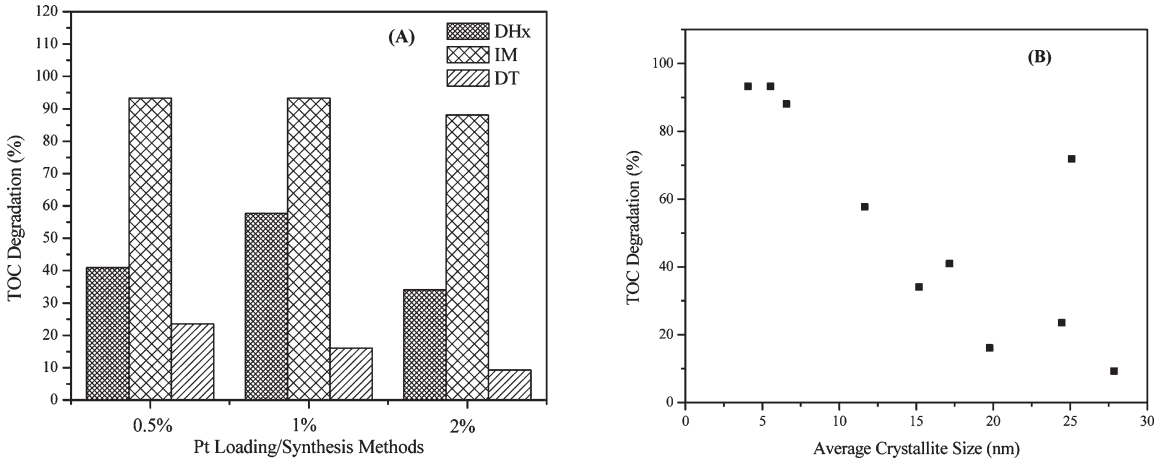

Figure 6. Evaluation of the photocatalytic activity of Pt−TiO_2−SiO_2 materials by TOC analysis. The materials were Pt-loaded with 0.5, 1, and 2 wt % using the direct DHxCR, template DTCR, and the impregnation (IMCR) method. Panel A shows the TOC activity at each loading and panel B indicates the effect of the crystallite size for the methods utilized in this study.

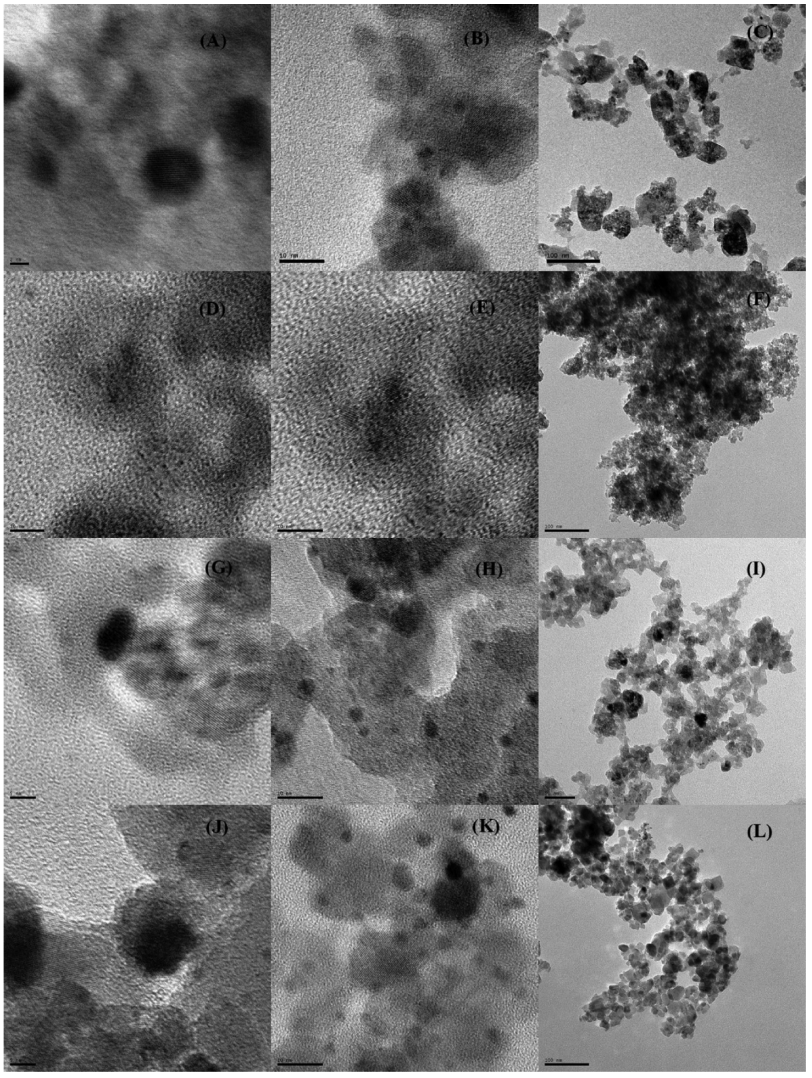

Figure 7. TEM images of Pt−TiO_2−SiO_2 materials prepared at 2 wt % Pt loadings: (A−C) synthesized by the direct DHxCR, (D−F) template DTCR, and (G−I) the impregnation (IMCR) method. Images for SiO_2-free Pt−TiO_2-2% are shown for comparison (J−L). The bar scales are 5, 10, and 100 nm from left to right.

dx.doi.org/10.1021/jp209620j |*J. Phys. Chem. C* 2011, 115, 25568–25579

Scheme 2. Proposed Reaction Mechanism for the Degradation of Phenol in an Oxygenated Environment Using Pt−TiO_2−SiO_2 Mixed Oxides and Detected by HPLC[a]

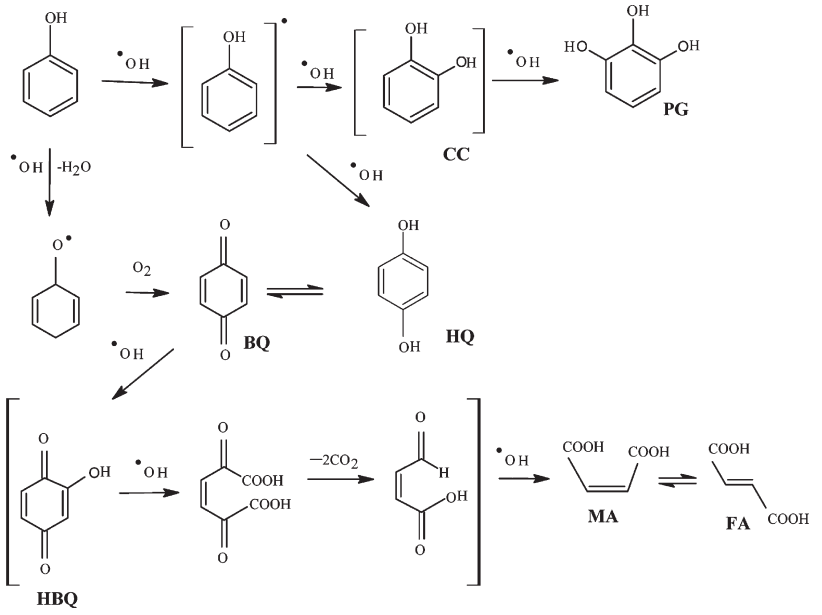

[a] Molecules shown in parentheses are postulated intermediates that have not been detected in the HPLC experiments in this study.

method results in materials of particles sizes within a definite range, the high activity in IMCR can be attributed to the small particle sizes of Pt dispersed on the surface of the mesostructure, as depicted by the plot in the Figure 6B.

Although the SiO_2 free Pt−TiO_2-2% has a large average crystallite size of Pt = 25 nm, the degradation efficiency is fairly high at 72%. The XRD pattern of this material shown in Figure 1 suggests the presence of mixed phases of anatase and rutile, thus implying different photodynamics compared with the other materials that contain the anatase phase only. The contribution of Pt is minimal on the photocatalytic activity because the two-phase composition already provides an efficient suppression of recombination due to an existing junction between anatase and rutile. The degradation efficiency of Pt−TiO_2-2% is still inferior to that of the Pt-mixed oxide material prepared by the IMCR method due to the larger sized Pt competing with anatase for UV photons. This emphasizes the relevance of noble-metal-containing mixed oxide materials for environmental remediation by semiconductor photocatalysts.

3.2. Control of Pt Particle Size of Pt−TiO_2−SiO_2. TEM images of platinized TiO_2−SiO_2 mixed oxide materials prepared by the synthesis methods DHxCR, DTCR, and IMCR are shown in the Figure 7. Supported TiO_2 particles are randomly distributed in the SiO_2 phase as grayish grains and in some incidents appear as lattice fringes of 20−25 nm in diameter. The Pt particles are of an average of 2−8 nm and appear in close proximity to TiO_2 lattice fringes as small dark circular spots due to their higher electron density. The particle size for Pt on TiO_2 prepared by the IMCR method is in the range of 4−7 nm, which is in reasonable agreement with the crystallite size that is determined by the CO pulse chemisorption results. However, the sizes estimated by TEM images for the materials prepared by the other two methods (DHxCR and DTCR) are of lower diameters than indicated by CO pulse chemisorption. It is notable that we can gain control of the average particle sizes depending on the choice of synthesis method. For loadings less than 2%, the particle sizes for each synthesis method are achieved within a narrow range irrespective of the amount of Pt loaded. DHxCR, DTCR, and IMCR result in particle sizes in the range of 11−17, 19−28, and 4−7 nm, respectively. The dispersions and crystallite sizes of other materials in relation to their photocatalytic activity are summarized in Table 2. Lee and Choi[44] argue that the different catalytic behavior between the platinized samples in their study were owed to the different oxidation state of deposited Pt species and not the size of the Pt particles. However, if the materials are containing Pt of the same oxidation state, that is, if metallic Pt^0 are considered, then the particle size and Pt loading play significant roles in the photocatalytic activity, as determined in this study. CO chemisorption studies clearly indicate that our Pt−TiO_2−SiO_2 materials contain metallic Pt, as evidenced by the saturation peaks observed in the uptake of CO during pulse titration studies. In contrast, the unreduced Pt containing samples do not evidence any CO molecules chemisorbed, indicating that these samples constitute Pt ions rather than Pt in the metallic state.

3.3. Proposed Mechanistic Pathway for the Degradation of Phenol by Pt−TiO_2−SiO_2. The TOC results were also compared with the concentration of the resultant reaction intermediates detected by high-performance liquid chromatography (HPLC) (Scheme 2). These studies were carried out to provide better understanding of the kinetics and mechanistic pathways that yield mineralization of the toxic pollutant, phenol. The intermediates were identified by matching the relative retention times of external standards. The main intermediates detected in this study were: MA, FA, PG, HQ, and BQ. These compounds were eluted within ranges of retention times: 1.8 to 1.9, 3.15, 3.3 to 3.4, 3.6 to 3.8, and 3.9 to 4.2 min, respectively, allowing for their easy and unambiguous identification. Various reactive oxidative species are produced during the photocatalysis process such as $O_2^{\bullet-}$, $^{\bullet}OH$, $^{\bullet}OOH$, HOOH, and OH^-.[6,45]

Among these, it is widely believed that the $^{\bullet}OH$ radical species are responsible for initiating the degradation events. These highly reactive species have an oxidation potential of 2.8 eV[46] and are known to be the most active reactive species for the mineralization process in the presence of oxygen.[47,48] When anatase TiO_2 comes into contact with Pt particles, a diffusion gradient is created due to the high affinity of Pt for electrons. This results in a charge separation between the conduction band electrons (e_{cb}^-) and holes (h_{vb}^+).[11] Subsequent transfer of photogenerated electrons to O_2 adsorbed onto the Pt−TiO_2 surface forms superoxide radicals ($O_2^{\bullet -}$) that will react with protons to form more $^{\bullet}OH$ radicals, as illustrated in the equation below.

$$O_2(ads) + e^- \rightarrow O_2^{-\bullet} \xrightarrow{H^+} {}^{\bullet}O_2H \xrightarrow{{}^{\bullet}O_2H} O_2 + H_2O_2 \xrightarrow{e^-} O_2 + {}^{\bullet}OH + HO^-$$

The mechanism also suggests that scavenging of conduction band electrons by O_2 increases the hole lifetime, thus allowing the holes to react with organic pollutant substrates.[49] The $^{\bullet}OH$ radicals produced attack the phenyl ring forming hydroxy phenyl radicals ($^{\bullet}PhOH$) and phenoxyl radicals ($PhO^{\bullet}$), short-lived radical intermediates detected by electron paramagnetic resonance spin trapping[50] and pulse radiolysis studies[51] of aqueous phenol, respectively. Despite the complexity of these highly reactive systems, it is reasonable to believe that $^{\bullet}PhOH$ may follow either a HQ or a CC pathway or concomitantly, and $PhO^{\bullet}$ proceeds through a BQ pathway depending on the mesostructure of the materials. The nature of the metal ions present in the mesostructure will determine the reaction pathway and the overall rate of the reaction.

The reaction intermediates resulting from the degradation by unplatinized TiO_2−SiO_2 were determined to be CC and hydroxybenzoquinone (HBQ), which emerged at retention times of 3.5 and 3.7, respectively. It is likely that the absence of Pt leads to an alternative reaction pathway that is fairly slower and allows for the detection and identification of more intermediates. Subsequent attacks of $^{\bullet}OH$ radicals on the $^{\bullet}PhOH$ radical may result in the formation of an unstable CC that rapidly yields PG. This intermediate is detected in all samples prepared in this study. However, the absence of Pt may slow down the reaction and produce a stable CC that is detected only in the unplatinized TiO_2−SiO_2 (not shown). We also established that the phenol degradation reaction by platinized TiO_2−SiO_2 mixed oxides proceeds through the HQ pathway. HQ is formed when the attack of a $^{\bullet}OH$ radical takes place in the para position. HQ can then be oxidized to BQ, which is further oxidized to unstable HBQ by the attack of a second $^{\bullet}OH$ radical.[52] BQ may also be formed from the oxidation of the $PhO^{\bullet}$ radical. It is imperative to note that the absence of the SiO_2 phase results in an enhancement in the amount of BQ generated, and this is in agreement with existing literature.[10] This marks the beginning of the production of acyclic compounds when the attack of another $^{\bullet}OH$ radical leads to ring cleavage forming 2,5-dioxo-3-hexenedioc acid, and the loss of CO_2 favors unsaturated 4-oxo-2-butenoic acid.[53] These rapid reactions result into MA present in equilibrium with FA, and complete mineralization may be rapidly achieved thereafter to form CO_2 and H_2O. The stable intermediates were detected in this study in less than 1 h of irradiation of all Pt−TiO_2−SiO_2 materials investigated in this study. It is noteworthy that complete mineralization was achieved with all materials prepared by the IMCR method in less than 30 min of irradiation, as suggested by the concentration values shown in Table 2. This high activity can be attributed to the high dispersion of small crystallite size Pt species in the mesostructure that minimizes the recombination of charge carriers.

4. CONCLUSIONS

Three different methods were employed to platinize TiO_2−SiO_2 successfully including the direct, template, and impregnation methods. Of these, the materials prepared by the impregnation method (IMCR) demonstrated very high photocatalytic activity of phenol with TOC degradation efficiencies of >90% in the as little as 30 min of irradiation under solar simulated conditions. This study accentuates the role of crystallite size of Pt as the main contributor to photocatalytic activity. The materials of the smaller particle sizes resulted in higher phenol degradation efficiencies regardless of the synthesis method employed. The proposed mechanism of this degradation process ensues primarily through the HQ pathway and through a small contribution from the CC pathway due to the formation of the highly unstable hydroxy phenyl radical. A significant portion of the mechanism may also proceed through the BQ pathway owing to the formation of the unstable phenoxyl radical.

AUTHOR INFORMATION

Corresponding Author

*E-mail: Harrison.Kibombo@usd.edu (H.S.K); Ranjit.Koodali@usd.edu. Tel: 605-677-6189. Fax: 605-677-6397.

ACKNOWLEDGMENT

We extend sincere gratitude to NSF-CHE-0619190, NSF-CHE-0722632, NSF-CHE-0840507, NSF-EPS-0903804, DE-FG02-08ER64624, Sigma Xi-G20101015154662, and the State of South Dakota for funding this project. We also thank Dr. Cuikun Lin for assistance with TEM studies and the International Precious Metals Institute (IPMI) Student Award 2010.

REFERENCES

(1) Young, J. A. Phenol. *J. Chem. Educ.* **2007**, *84*, 759–759.

(2) Keith, L.; Telliard, W. ES&T special report: priority pollutants: I-A perspective view. *Environ. Sci. Technol.* **1979**, *13*, 416–423.

(3) Michałowicz, J.; Duda, W. Phenols - sources and toxicity. *Pol. J. Environ. Stud.* **2007**, *16*, 347–362.

(4) Hayashi, M.; Nakamura, Y.; Higashi, K.; Kato, H.; Kishida, F.; Kaneko, H. A quantitative structure-activity relationship study of the skin irritation potential of phenols. *Toxicol. In Vitro* **1999**, *13*, 915–922.

(5) Davis, M. E. Ordered porous materials for emerging applications. *Nature* **2002**, *417*, 813–821.

(6) Linsebigler, A. L.; Lu, G.; Yates, J. T. Photocatalysis on TiO_2 surfaces: principles, mechanisms, and selected results. *Chem. Rev.* **1995**, *95*, 735–758.

(7) (a) Ranjit, K. T.; Varadarajan, T. K.; Viswanathan, B. Photocatalytic reduction of dinitrogen to ammonia over noble-metal-loaded TiO_2. *J. Photochem. Photobiol., A* **1996**, *96*, 181–185. (b) Ishitani, O.; Inoue, C.; Suzuki, Y.; Ibusuki, T. Photocatalytic reduction of carbon dioxide to methane and acetic acid by an aqueous suspension of metal-deposited TiO_2. *J. Photochem. Photobiol., A* **1993**, *72*, 269–271.

(8) Chen, H.-W.; Ku, Y.; Kuo, Y.-L. Effect of Pt/TiO_2 characteristics on temporal behavior of *o*-cresol decomposition by visible light-induced photocatalysis. *Water Res.* **2007**, *41*, 2069–2078.

(9) Zhang, F.; Chen, J.; Zhang, X.; Gao, W.; Jin, R.; Guan, N.; Li, Y. Synthesis of titania-supported platinum catalyst: the effect of pH on morphology control and valence state during photodeposition. *Langmuir* **2004**, *20*, 9329–9334.

(10) Emilio, C. A.; Litter, M. I.; Kunst, M.; Bouchard, M.; Colbeau-Justin, C. Phenol photodegradation on platinized-TiO_2 photocatalysts related to charge-carrier dynamics. *Langmuir* **2006**, *22*, 3606–3613.

(11) Sun, B.; Smirniotis, P. G.; Boolchand, P. Visible light photocatalysis with platinized rutile TiO_2 for aqueous organic oxidation. *Langmuir* **2005**, *21*, 11397–11403.

(12) Gao, X.; Wachs, I. E. Titania-silica as catalysts: molecular structural characteristics and physico-chemical properties. *Catal. Today* **1999**, *51*, 233–254.

(13) Kang, C.; Jing, L.; Guo, T.; Cui, H.; Zhou, J.; Fu, H. Mesoporous SiO_2-modified nanocrystalline TiO_2 with high anatase thermal stability and large surface area as efficient photocatalyst. *J. Phys. Chem. C* **2008**, *113*, 1006–1013.

(14) Miller, J. B.; Ko, E. I. Control of mixed oxide textural and acidic properties by the sol-gel method. *Catal. Today* **1997**, *35*, 269–292.

(15) Dagan, G.; Sampath, S.; Lev, O. Preparation and utilization of organically modified silica-titania photocatalysts for decontamination of aquatic environments. *Chem. Mater.* **1995**, *7*, 446–453.

(16) Wang, C.-C.; Ying, J. Y. Sol−gel synthesis and hydrothermal processing of anatase and rutile titania nanocrystals. *Chem. Mater.* **1999**, *11*, 3113–3120.

(17) Pabón, E. TiO_2−SiO_2 mixed oxides prepared by a combined sol−gel and polymer inclusion method. *Microporous Mesoporous Mater.* **2004**, *67*, 195–203.

(18) Coles, M. P.; Lugmair, C. G.; Terry, K. W.; Tilley, T. D. Titania−silica materials from the molecular precursor $Ti[OSi(OtBu)_3]_4$: selective epoxidation catalysts. *Chem. Mater.* **1999**, *12*, 122–131.

(19) Rupp, W.; Husing, N.; Schubert, U. Preparation of silica-titania xerogels and aerogels by sol-gel processing of new single-source precursors. *J. Mater. Chem.* **2002**, *12*, 2594–2596.

(20) Davis, R. J.; Liu, Z. Titania−silica: a model binary oxide catalyst system. *Chem. Mater.* **1997**, *9*, 2311–2324.

(21) Li, Y.; Kim, S.-J. Synthesis and characterization of nano titania particles embedded in mesoporous silica with both high photocatalytic activity and adsorption capability. *J. Phys. Chem. B* **2005**, *109*, 12309–12315.

(22) Kibombo, H. S.; Zhao, D.; Gonshorowski, A.; Budhi, S.; Koppang, M. D.; Koodali, R. T. Cosolvent-induced gelation and the hydrothermal enhancement of the crystallinity of titania−silica mixed oxides for the photocatalytic remediation of organic pollutants. *J. Phys. Chem. C* **2011**, *115*, 6126–6135.

(23) Herrmann, J. M. Heterogeneous photocatalysis: state of the art and present applications in honor of Pr. R.L. Burwell Jr. (1912−2003), former head of Ipatieff Laboratories, Northwestern University, Evanston (Ill). *Top. Catal.* **2005**, *34*, 49–65.

(24) Fox, M. A.; Dulay, M. T. Heterogeneous photocatalysis. *Chem. Rev.* **1993**, *93*, 341–357.

(25) Garcia-Martinez, J.; Linares, N.; Sinibaldi, S.; Coronado, E.; Ribera, A. Incorporation of Pd nanoparticles in mesostructured silica. *Microporous Mesoporous Mater.* **2009**, *117*, 170–177.

(26) Kruk, M.; Jaroniec, M. Gas adsorption characterization of ordered organic−inorganic nanocomposite materials. *Chem. Mater.* **2001**, *13*, 3169–3183.

(27) Lowell, S. S., J. E.; Thomas, M. A.; Thommes, M. *Characterization of Porous Solids and Powders: Surface Area, Pore Size and Density*; Academic Press: San Diego, 1990; Vol. 13.

(28) Dallaporta, H.; Liehr, M.; Lewis, J. E. Silicon dioxide defects induced by metal impurities. *Phys. Rev. B* **1990**, *41*, 5075–5083.

(29) Yu, R.; Song, H.; Zhang, X.-F.; Yang, P. Thermal wetting of platinum nanocrystals on silica surface. *J. Phys. Chem. B* **2005**, *109*, 6940–6943.

(30) Reddy, B. M.; Manohar, B.; Reddy, E. P. Oxygen chemisorption on titania-zirconia mixed oxide supported vanadium oxide catalysts. *Langmuir* **1993**, *9*, 1781–1785.

(31) Reddy, B.; Rao, K.; Reddy, G. Controlled hydrogenation of acetophenone over Pt/CeO_2−MO_x (M = Si, Ti, Al, and Zr) catalysts. *Catal. Lett.* **2009**, *131*, 328–336.

(32) Domen, K.; Sakata, Y.; Kudo, A.; Maruya, K.-i.; Onishi, T. The photocatalytic activity of a platinized titanium dioxide catalyst supported over silica. *Bull. Chem. Soc. Jpn.* **1988**, *61*, 359–362.

(33) Zeitler, V. A.; Brown, C. A. The infrared spectra of some Ti-O-Si, Ti-O-Ti, and Si-O-Si compounds. *J. Phys. Chem.* **1957**, *61*, 1174–1177.

(34) Dirken, P. J.; Smith, M. E.; Whitfield, H. J. ^{17}O and ^{29}Si solid state NMR study of atomic scale structure in sol-gel-prepared TiO_2-$Si0_2$ materials. *J. Phys. Chem.* **1995**, *99*, 395–401.

(35) Handy, B. E.; Maciejewski, M.; Baiker, A.; Wokaun, A. Genesis and structural properties of alkoxide-prepared titania-silica xerogels. *J. Mater. Chem.* **1992**, *2*, 833–840.

(36) Ren, J.; Li, Z.; Liu, S.; Xing, Y.; Xie, K. Silica−titania mixed oxides: Si−O−Ti connectivity, coordination of titanium, and surface acidic properties. *Catal. Lett.* **2008**, *124*, 185–194.

(37) Tanaka, K.; Miyahara, K.; Toyoshima, I. Adsorption of carbon dioxide on titanium dioxide and platinum/titanium dioxide studied by X-ray photoelectron spectroscopy and auger electron spectroscopy. *J. Phys. Chem.* **1984**, *88*, 3504–3508.

(38) Benvenutti, E. V.; Franken, L.; Moro, C. C.; Davanzo, C. U. FTIR study of hydrogen and carbon monoxide adsorption on Pt/TiO_2, Pt/ZrO_2, and Pt/Al_2O_3. *Langmuir* **1999**, *15*, 8140–8146.

(39) Ohtani, B.; Iwai, K.; Nishimoto, S.-i.; Sato, S. Role of platinum deposits on titanium(IV) oxide particles: structural and kinetic analyses of photocatalytic reaction in aqueous alcohol and amino acid solutions. *J. Phys. Chem. B* **1997**, *101*, 3349–3359.

(40) Xu, J.; Li, L.; Yan, Y.; Wang, H.; Wang, X.; Fu, X.; Li, G. Synthesis and photoluminescence of well-dispersible anatase TiO_2 nanoparticles. *J. Colloid Interface Sci.* **2008**, *318*, 29–34.

(41) Sánchez, E.; López, T.; Gómez, R.; Bokhimi, H.; Morales, A.; Novaro, O. Synthesis and characterization of sol−gel Pt/TiO_2 catalyst. *J. Solid State Chem.* **1996**, *122*, 309–314.

(42) Ryczkowski, J. IR spectroscopy in catalysis. *Catal. Today* **2001**, *68*, 263–381.

(43) Sun, B.; Vorontsov, A. V.; Smirniotis, P. G. Role of platinum deposited on TiO_2 in phenol photocatalytic oxidation. *Langmuir* **2003**, *19*, 3151–3156.

(44) Lee, J.; Choi, W. Photocatalytic reactivity of surface platinized TiO_2: substrate specificity and the effect of Pt oxidation state. *J. Phys. Chem. B* **2005**, *109*, 7399–7406.

(45) Li, X.; Cubbage, J. W.; Jenks, W. S. Photocatalytic degradation of 4-chlorophenol. 2. The 4-chlorocatechol pathway. *J. Org. Chem.* **1999**, *64*, 8525–8536.

(46) Kommineni, S.; Zoeckler, J.; Stocking, A. J.; Liang, S.; Flores, A. E.; Kavanaugh, M. C. *Advanced Oxidation Processes*; National Water Research Institute: Fountain Valley, CA, 2000; pp 111−208.

(47) Turchi, C. S.; Ollis, D. F. Photocatalytic degradation of organic water contaminants: mechanisms involving hydroxyl radical attack. *J. Catal.* **1990**, *122*, 178–192.

(48) Guo, Z.; Ma, R.; Li, G. Degradation of phenol by nanomaterial TiO_2 in wastewater. *Chem. Eng. J.* **2006**, *119*, 55–59.

(49) Tasbihi, M.; Ngah, C. R.; Aziz, N.; Mansor, A.; Abdullah, A. Z.; Teong, L. K.; Mohamed, A. R. Lifetime and regeneration studies of various supported TiO_2 photocatalysts for the degradation of phenol under UV-C light in a batch reactor. *Ind. Eng. Chem. Res.* **2007**, *46*, 9006–9014.

(50) Theurich, J.; Lindner, M.; Bahnemann, D. W. Photocatalytic degradation of 4-chlorophenol in aerated aqueous titanium dioxide suspensions: a kinetic and mechanistic study. *Langmuir* **1996**, *12*, 6368–6376.

(51) Land, E. J.; Ebert, M. Pulse radiolysis studies of aqueous phenol. Water elimination from dihydroxycyclohexadienyl radicals to form phenoxyl. *Trans. Faraday Soc.* **1967**, *63*, 1181–1190.

(52) Theurich, J.; Lindner, M.; Bahnemann, D. W. Photocatalytic degradation of 4-chlorophenol in aerated aqueous titanium dioxide suspensions: a kinetic and mechanistic study. *Langmuir* **1996**, *12*, 6368–6376.

(53) Devlin, H. R.; Harris, L. J. Mechanism of the oxidation of aqueous phenol with dissolved oxygen. *Ind. Eng. Chem. Fundam.* **1984**, *23*, 387–392.